JCI insight

RESEARCH ARTICLE

# Epigenetic programming of estrogen receptor in adipocytes by high-fat diet regulates obesity-induced inflammation

**Rui Wu,[1,2] Fenfen Li,[2] Shirong Wang,[2] Jia Jing,[2] Xin Cui,[2] Yifei Huang,[2] Xucheng Zhang,[2] Jose A. Carrillo,[3] Zufeng Ding,[2] Jiuzhou Song,[3] Liqing Yu,[4] Huidong Shi,[5,6] Bingzhong Xue,[2] and Hang Shi[2]**

[1]School of Pharmaceutical Science and Technology, Hangzhou Institute for Advanced Study, University of Chinese Academy of Sciences, Hangzhou, China. [2]Department of Biology, Georgia State University, Atlanta, Georgia, USA. [3]Department of Animal and Avian Sciences, University of Maryland at College Park, College Park, Maryland, USA. [4]Division of Endocrinology, Diabetes and Nutrition, Department of Medicine, University of Maryland School of Medicine, Baltimore, Maryland, USA. [5]Georgia Cancer Center and [6]Department of Biochemistry and Molecular Biology, Medical College of Georgia, Augusta University, Augusta, Georgia, USA.

**Adipose inflammation plays a key role in obesity-induced metabolic abnormalities. Epigenetic regulation, including DNA methylation, is a molecular link between environmental factors and complex diseases. Here we found that high-fat diet (HFD) feeding induced a dynamic change of DNA methylome in mouse white adipose tissue (WAT) analyzed by reduced representative bisulfite sequencing. Interestingly, DNA methylation at the promoter of estrogen receptor α (*Esr1*) was significantly increased by HFD, concomitant with a downregulation of *Esr1* expression. HFD feeding in mice increased the expression of DNA methyltransferase 1 (*Dnmt1*) and *Dnmt3a* and binding of DNMT1 and DNMT3a to *Esr1* promoter in WAT. Mice with adipocyte-specific *Dnmt1* deficiency displayed increased *Esr1* expression, decreased adipose inflammation, and improved insulin sensitivity upon HFD challenge; mice with adipocyte-specific *Dnmt3a* deficiency showed a mild metabolic phenotype. Using a modified CRISPR/RNA-guided system to specifically target DNA methylation at the *Esr1* promoter in WAT, we found that reducing DNA methylation at *Esr1* promoter increased *Esr1* expression, decreased adipose inflammation, and improved insulin sensitivity in HFD-challenged mice. Our study demonstrated that DNA methylation at *Esr1* promoter played an important role in regulating adipose inflammation, which may contribute to obesity-induced insulin resistance.**

## Introduction

Obesity is characterized by chronic inflammation that causally links obesity to insulin resistance/type 2 diabetes (1, 2). Adipose tissue plays a key role in the generation of inflammatory response and mediators in obesity (1, 2). Inflammatory signaling pathways in fat tissue can be activated in nutrient-rich conditions (3). However, it is still not fully understood how the inflammatory program is altered by nutrient-rich conditions that often promote obesity.

Since the original reports linking chronic inflammation in adipose tissue to obesity-induced insulin resistance, there have been numerous publications studying pathways underlying obesity-induced inflammation in metabolic dysfunctions (2). While most studies have been devoted to the evaluation of genetic pathways (e.g., ER stress, oxidative stress, ceramide formation) that mediate nutrient-induced abnormalities in metabolic tissues (2), much less is known about epigenetic mechanisms, a link between environmental factors (e.g., diets) and complex diseases (e.g., obesity and diabetes), in this process. One of the most common epigenetic regulations is DNA methylation of cytosines at mainly CpG dinucleotides, which frequently takes place in the promoter and 5′ regions of genes (4). DNA hypomethylation at gene promoters often results in transcriptional activation, while hypermethylation is often associated with gene silencing (4). De novo DNA

**Conflict of interest:** The authors have declared that no conflict of interest exists.



**Submitted:** June 27, 2023
**Accepted:** August 20, 2025
**Published:** August 26, 2025

**Reference information:** *JCI Insight*. 2025;10(19):e173423. https://doi.org/10.1172/jci.insight.173423.

methylation is mediated by DNA methyltransferase (DNMT) 3a and 3b. Once established, DNA methylation is then maintained through mitosis primarily by the maintenance enzyme DNMT1 (5, 6). However, recent evidence also supported a role of DNMT1 in de novo DNA methylation (7). On the other hand, DNA demethylation can be achieved by the ten-eleven translocation 1 (TET1) dioxygenase that catalyzes the hydroxylation of 5-methylcytosine (5-mC) to 5-hydroxymethylcytosine and subsequent generation of 5-formylcytosine and 5-carboxylcytosine, which are then converted to unmodified cysteines by replication-related dilution or glycosylation-mediated base-excision repair (8, 9). The key role of DNA methylation and its maintenance enzyme DNMT1 in metabolic inflammation has been revealed in our recent report demonstrating that hypermethylation at peroxisome proliferator activated receptor γ (*Pparγ*) promoter by saturated fatty acids and pro-inflammatory cytokines, levels of which are commonly elevated in obesity, promotes M1 pro-inflammatory macrophage polarization and inflammation in adipose tissue, resulting in insulin resistance in obesity (10). However, it is not clear whether and how DNA methylation plays a role in adipocyte chemotaxis and inflammation, an integral part of overall adipose inflammation.

In the present study, we tested the hypothesis that DNA methylation at estrogen receptor α (*Esr1*) promoter mediates adipocyte inflammation and chemotaxis, leading to obesity-induced insulin resistance. Using reduced representation bisulfite sequencing (RRBS) analysis, we conducted a genome-wide profiling of DNA methylation in adipose tissue of diet-induced obese (DIO) mice. From the RRBS analysis, we discovered a significant increase in DNA methylation at *Esr1* promoter, which is associated with downregulation of *Esr1* expression. We also found that *Esr1* promoter activity was differentially regulated in unmethylated versus methylated state. Using ChIP assays, we found an increased binding of DNMT1 and DNMT3a to the *Esr1* promoter in white adipose tissue of mice fed high-fat diet (HFD). We then generated adipocyte-specific *Dnmt1* and *-3a* knockout (AD1KO and AD3aKO) mice and characterized their inflammatory status and metabolic phenotypes. Finally, we used a CRISPR/RNA-guided system to specifically induce methylation/demethylation at the *Esr1* promoter and further characterized adipocyte inflammation/chemotaxis, macrophage infiltration, and insulin sensitivity in these mice challenged with HFD feeding.

## Results

*Dynamic changes of the DNA methylome in white fat of HFD-fed mice*. To study whether HFD reprograms the DNA methylome in fat tissue, we performed a DNA methylation profiling experiment in gonadal white adipose tissue (gWAT) of male mice fed with either low-fat diet (LFD) or HFD for 12 weeks using the RRBS approach (11–13). Our bioinformatic analysis showed that there were up to 1,630 differentially methylated regions (DMRs) in HFD- versus chow-fed mice. Around 44.1% of the DMRs were located in intergenic regions, with the rest of the DMRs distributed within genes including 5′-end/5′-untranslated region (5′-UTR), cDNA coding sequences (CDS), introns, and 3′-end/3′-UTR (Figure 1A). Within the genes with altered DNA methylation level, 700 genes exhibited upregulated DNA methylation rates by HFD and 211 genes exhibited downregulated DNA methylation rates by HFD. These data suggest that HFD feeding dynamically changes DNA methylome in fat, with the majority of the genes (77%) exhibiting an increase in DNA methylation status. In addition, Gene Ontology (GO) and Kyoto Encyclopedia of Genes and Genomes (KEGG) analysis suggested that genes with methylation changes were involved in various pathways, including biological process, molecular function, and cellular component (Supplemental Figure 1; supplemental material available online with this article; https://doi.org/10.1172/jci.insight.173423DS1).

*Methylation of the Esr1 promoter is enhanced by HFD feeding possibly via DNMT1 and DNMT3a*. Notably, our RRBS profiling indicated that methylation rate at the 5′-end of the *Esr1* promoter was significantly increased in gWAT of HFD-fed mice as indicated using the University of California Santa Cruz (UCSC) Genome Browser (Figure 1B). Since adipocyte *Esr1* has emerged as an antiinflammatory molecule in obesity (14–16), we focus on *Esr1* as the main methylation target during diet-induced obesity in this study. Interestingly, the proximal promoter and 5′-UTR of *Esr1* are enriched with CpG islands, among which 5 CpG sites are located downstream adjacent to the TATA box (Supplemental Figure 2), raising a possibility that the *Esr1* promoter might be subjected to epigenetic regulation through DNA methylation by HFD. Indeed, our pyrosequencing analysis indicated that HFD feeding significantly increased DNA methylation at several CpG sites at *Esr1* promoter in gWAT of male C57BL6J mice (Figure 1C). In consistency, the average DNA methylation rate at *Esr1* promoter in gWAT was increased in both 12-week and 24-week HFD-fed mice (Figure 1D). This was associated with downregulation of *Esr1* mRNA expression in gWAT of both 12-week and 24-week HFD-fed mice, with a more profound

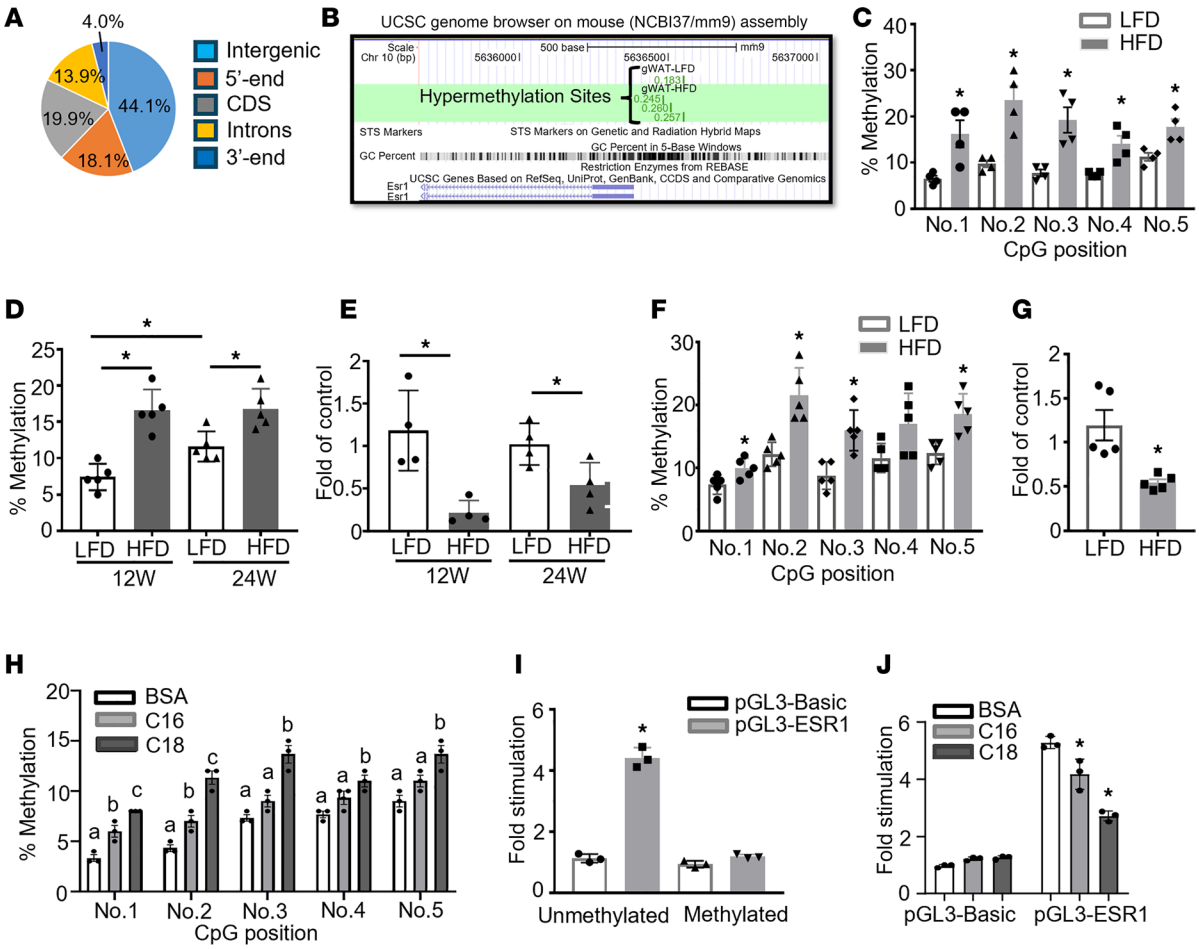


**Figure 1. HFD regulates *Esr1* expression via promoter DNA methylation.** (**A** and **B**) Distribution of DMRs in the genome (**A**) and RRBS profiling of DNA methylation levels at *Esr1* promoter (**B**) in gWAT of male mice fed with LFD or HFD for 12 weeks. RRBS was performed in gWAT from male C57BL/6J mice fed with LFD or HFD for 12 weeks. Genomic DNA from 4 animals was pooled in each group for RRBS analysis. (**C**) DNA methylation levels at individual CpG sites at *Esr1* promoter in gWAT of male C57BL/6J mice fed LFD or HFD for 12 weeks, $n = 4$/group. *$P < 0.05$ vs. LFD by Student's *t* test. (**D** and **E**) Average DNA methylation levels at *Esr1* promoter (**D**, $n = 5$/group) and *Esr1* expression (**E**, $n = 4$/group) in gWAT of male C57BL/6J mice fed LFD or HFD for 12 or 24 weeks. *$P < 0.05$ vs. LFD by Student's *t* test. (**F** and **G**) DNA methylation levels at individual CpG sites at *Esr1* promoter (**F**) and *Esr1* expression (**G**) in gWAT of female C57BL/6J mice fed LFD or HFD for 12 weeks, $n = 5$/group. *$P < 0.05$ vs. LFD by Student's *t* test. (**H**) DNA methylation levels at individual CpG sites at *Esr1* promoter in 3T3-L1 adipocytes treated with palmitate (C16) or stearate (C18), $n = 3$/group. Groups labeled with different letters are statistically different from each other as analyzed by 1-way ANOVA with Fisher's least significant difference (LSD) post hoc test. (**I**) *Esr1* promoter luciferase activity in 3T3-L1 adipocytes transfected with fully methylated or unmethylated constructs, $n = 3$. *$P < 0.05$ vs. all other groups as analyzed by 2-way ANOVA with Fisher's LSD post hoc test. (**J**) *Esr1* promoter luciferase activity in 3T3-L1 adipocytes transfected with unmethylated constructs treated with BSA, palmitate (C:16, 200 μM), or stearate (C:18, 200 μM). $n = 3$. *$P < 0.05$ vs. BSA by 2-way ANOVA with Fisher's LSD post hoc test. All data are expressed as mean ± SEM.

reduction observed in 12-week HFD-fed mice (Figure 1E). Interestingly, we observed that average DNA methylation level at *Esr1* promoter was already increased in 24-week LFD-fed mice compared with that of 12-week (Figure 1D), suggesting that besides dietary factors, aging may be another important factor that regulates DNA methylation at *Esr1* promoter, which may contribute to aging-associated metabolic dysfunction. This age-related change may contribute to the more profoundly increased *Esr1* promoter DNA methylation and more profoundly reduced *Esr1* expression observed between HFD- and LFD-fed mice at 12 weeks compared with that of 24 weeks (Figure 1, D and E). Similarly, we also found that HFD-fed female mice, like male mice, also displayed increased DNA methylation rate at *Esr1* promoter coupled with decreased *Esr1* expression in the gonadal fat depots (gWAT) (Figure 1, F and G).

We then tested whether saturated free fatty acids, whose levels are abundant in HFDs and are commonly elevated in obesity, regulate DNA methylation levels at the *Esr1* promoter. 3T3-L1 preadipocytes were differentiated and treated with palmitate (C16, 200 μM) and stearate (C18, 200 μM) for 2 days. Pyrosequencing analysis showed that stearate significantly upregulated methylation rates at individual CpG sites at *Esr1* promoter, while palmitate exerted a lesser effect (Figure 1H). To determine whether *Esr1* promoter activity is indeed regulated by

methylation, we cloned a 1 kb proximal promoter region at the *Esr1* locus, including the CpG-enriched regions, into pGL3-luciferase expression vector and examined the fully methylated versus unmethylated *Esr1* promoter activity by transfecting these constructs into 3T3-L1 cells. Our luciferase assays showed that the luciferase activity of the unmethylated promoter was more than 4-fold higher than that of the fully methylated promoter (Figure 1I). Interestingly, the increased luciferase activity in unmethylated *Esr1* promoter was significantly suppressed in the presence of 200 μM palmitate or stearate (Figure 1J), further verifying that saturated fatty acids suppress *Esr1* promoter activity via regulating *Esr1* promoter DNA methylation.

To determine which DNA methyltransferases (DNMT1, 3A, or 3B) and demethylases (TET1, 2, and 3) may mediate the increased DNA methylation at the *Esr1* promoter caused by HFD feeding, we examined the binding of DNMTs to the *Esr1* promoter using ChIP assay in gWAT of mice fed with either LFD or HFD. We found that HFD feeding significantly enhanced the binding of DNMT1 and DNMT3A to the *Esr1* promoter in gWAT (Figure 2, A and B), while we could not detect any DNMT3B binding to *Esr1* promoter because of low expression (data not shown). Interestingly, HFD feeding also increased mRNA expression of *Dnmt1* and *Dnmt3a* in gWAT of HFD-fed mice (Figure 2, C and D). A similar increase was also observed in DNMT1 protein levels in gWAT of HFD-fed mice (Figure 2E). Moreover, HFD feeding also downregulated the expression of *Tet1* and *Tet2* and tended to downregulate *Tet3* expression in gWAT (Supplemental Figure 3). To further narrow down whether DNMT1 or -3A mediates *Esr1* promoter methylation, we knocked down *Dnmt1* or *Dnmt3a* in 3T3-L1 adipocytes after day 5 or day 8 of differentiation. We found that *Dnmt1* knockdown markedly promoted the expression of *Esr1* mRNA in adipocytes with *Dnmt1* knockdown at either day 5 or day 8 of differentiation, while *Dnmt3a* knockdown either had no effect on or even decreased *Esr1* expression (Figure 2, F and G). To further study how *Dnmt1* regulates *Esr1* expression in more physiologically relevant settings, we generated AD1KO mice by crossing *Dnmt1*-floxed mice (17) with adiponectin-Cre mice (18). We found that adipocytes differentiated from AD1KO mice significantly increased the expression of *Esr1* compared with adipocytes differentiated from fl/fl mice (Figure 2H). These data suggest that DNMT1 may be a key enzyme in mediating *Esr1* promoter methylation induced by HFD feeding.

*Inhibiting DNA methylation increases Esr1 expression and decreases inflammation in adipocytes*. Since *Esr1* has been implicated in the regulation of inflammatory pathways (14–16), we interrogated whether inhibiting DNA methylation could increase *Esr1* expression, thereby decreasing inflammation in adipocytes. Indeed, knockdown of *Esr1* in 3T3-L1 adipocytes (Supplemental Figure 4A) promoted the expression of inflammatory genes, such as tumor necrosis factor (*Tnfα*) and interleukin-1β (*Il1β*) (Figure 3A), while overexpression of *Esr1* (Supplemental Figure 4B) significantly suppressed these inflammatory genes' expression (Figure 3B). We then investigated whether inhibiting DNA methylation pharmacologically by 5-aza-2′-deoxycytidine (5-aza-dC), a nucleoside-based DNMT inhibitor that induces demethylation, would cause demethylation at the *Esr1* promoter and increase its expression, leading to an antiinflammatory effect in adipose tissue. We fed 6-week-old male C57BL/6J mice with either LFD or HFD for 16 weeks to establish diet-induced obesity and then treated them with either saline or low-dose 5-aza-dC (i.p.) (0.25 mg/kg BW, 3 times per week) for 6 weeks. This low-dose 5-aza-dC treatment has been shown to exert very low toxicity as it did not change body weight and fat mass (10, 19). As expected, 5-aza-dC treatment did not change body weight and adiposity in these mice (Supplemental Figure 5, A–C). However, while 5-aza-dC treatment did not change fed glucose levels, it significantly reduced fed insulin levels, and calculated glucose × insulin products (Figure 3C), indicating 5-aza-dC treatment improved insulin sensitivity in HFD-fed mice without changes in body weight and adiposity. This was verified by ITT (Figure 3C). Interestingly, we found that HFD feeding suppressed the expression of *Esr1* in gWAT, which was restored by 5-aza-dC treatment (Figure 3D). Moreover, 5-aza-dC treatment prevented HFD-induced expression of inflammatory genes, such as *Tnfα* and *Il1β* (Figure 3D).

This was further verified with a genetic approach using *Dnmt1*-deficient adipocytes differentiated from primary preadipocytes of AD1KO. Primarily differentiated adipocytes from *Dnmt1*-deficient or fl/fl mice were treated with saturated fatty acids and pro-inflammatory cytokines, obesity-associated factors whose levels are commonly elevated in obesity. We found that the saturated fatty acids palmitate (C16) and stearate (C18) promoted inflammatory gene expression in adipocytes from fl/fl mice; this effect was prevented in adipocytes from AD1KO mice (Figure 4, A and B). Similar results were observed in *Dnmt1*-deficient adipocytes treated with TNF-α. *Dnmt1* deficiency significantly attenuated TNF-α–induced expression of inflammatory genes, including *Tnfα*, *Il6*, inducible nitric oxide synthase 2 (*Nos2*/*iNos*), and monocyte chemoattractant protein-1 (*Mcp1*) (Figure 4, C–F).

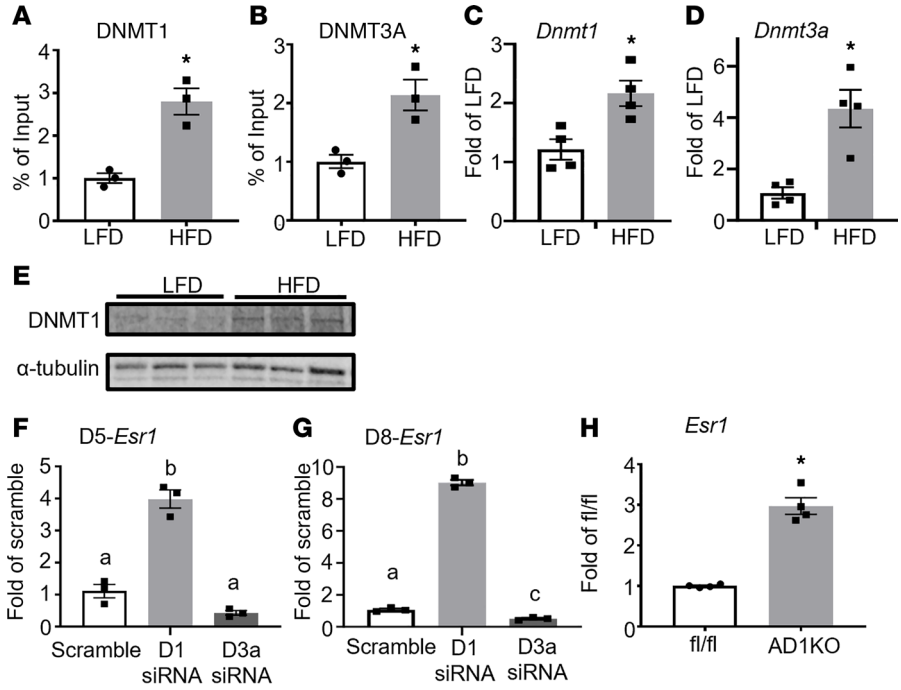


**Figure 2. DNMT1 mediates HFD-induced increase of DNA methylation at *Esr1* promoter.** (**A** and **B**) ChIP analysis of binding of DNMT1 (**A**) and DNMT3a (**B**) at *Esr1* promoter in gWAT of male mice fed with LFD or HFD for 12 weeks, $n = 3$/group. $^*P < 0.05$ vs. LFD by Student's $t$ test. (**C** and **D**) Expression of *Dnmt1* (**C**) and *Dnmt3a* (**D**) in gWAT of male mice fed with LFD or HFD for 12 weeks, $n = 4$/group. $^*P < 0.05$ vs. LFD by Student's $t$ test. (**E**) DNMT1 protein levels in gWAT of male mice fed with LFD or HFD for 12 weeks, $n = 3$/group. (**F** and **G**) Expression of *Esr1* in 3T3-L1 adipocytes with *Dnmt1* or *Dnmt3a* knockdown at day 5 (**F**) or day 8 (**G**) of differentiation, $n = 3$/group. Groups labeled with different letters are statistically different from each other as analyzed by 1-way ANOVA with Fisher's LSD post hoc test. (**H**) Expression of *Esr1* in primary adipocytes differentiated from AD1KO and their fl/fl littermates, $n = 4$/group. $^*P < 0.05$ vs. fl/fl by Student's $t$ test. All data are expressed as mean ± SEM.

We have previously shown that inhibiting DNA methylation in macrophages by 5-aza-dC or *Dnmt1* deficiency exerts significant antiinflammatory effects (10). To further study whether the beneficial effects of inhibiting DNA methylation with either 5-aza-dC or adipocyte-specific *Dnmt1* deletion are mediated via adipocyte *Esr1*, we knocked down both *Dnmt1* and *Esr1* in differentiated 3T3-L1 adipocytes. As shown in Figure 4, G–I, knocking down *Dnmt1* significantly increased *Esr1* expression in 3T3-L1 adipocytes, with the concomitant downregulation of *Tnfα* and *Il1β*. As expected, *Esr1* knockdown in 3T3-L1 adipocytes significantly upregulated *Tnfα* and *Il1β* expression and further abolished the inhibitory effects of *Dnmt1* knockdown on these pro-inflammatory cytokines' expression, indicating that the beneficial effects of inhibiting DNA methylation on adipose tissue are mediated by adipocyte *Esr1*.

*Adipocyte-specific deletion of DNA methylation ameliorates HFD-induced obesity, adipose inflammation, and insulin resistance*. To more specifically study the role of adipocyte *Dnmt1* in regulating adipose tissue inflammation, we generated AD1KO mice by crossing *Dnmt1*-floxed mice with adiponectin-Cre mice. As expected, *Dnmt1* mRNA and protein levels were decreased in gWAT of AD1KO mice (Supplemental Figure 6, A and B). We then further characterized the metabolic phenotypes of body weight, adipose inflammation, and insulin sensitivity in both female and male AD1KO and their control fl/fl littermate mice fed HFD. Figure 5A showed that upon challenge with HFD, there was no significant difference in body weight in female mice between the 2 genotypes. However, female AD1KO mice exhibited a significant decrease in fat mass in various fat depots (Figure 5B) with smaller adipocytes (Figure 5C), whereas no difference in liver weight was observed (Figure 5B). Using a PhenoMaster metabolic cage system, we found that female AD1KO mice exhibited higher energy expenditure (Figure 5D) with higher oxygen consumption (Supplemental Figure 6C) with no changes in locomotor activity and food intake (Supplemental Figure 6, D and E), suggesting that the enhanced energy expenditure in female AD1KO mice largely accounted for their reduced adiposity. Further, female AD1KO mice also displayed improved glucose tolerance and insulin sensitivity as assessed by glucose and insulin tolerance tests (Figure 5, E and F). These data indicate that female mice with adipocyte *Dnmt1* deficiency have reduced adiposity when fed HFD and are protected from obesity-induced insulin resistance.

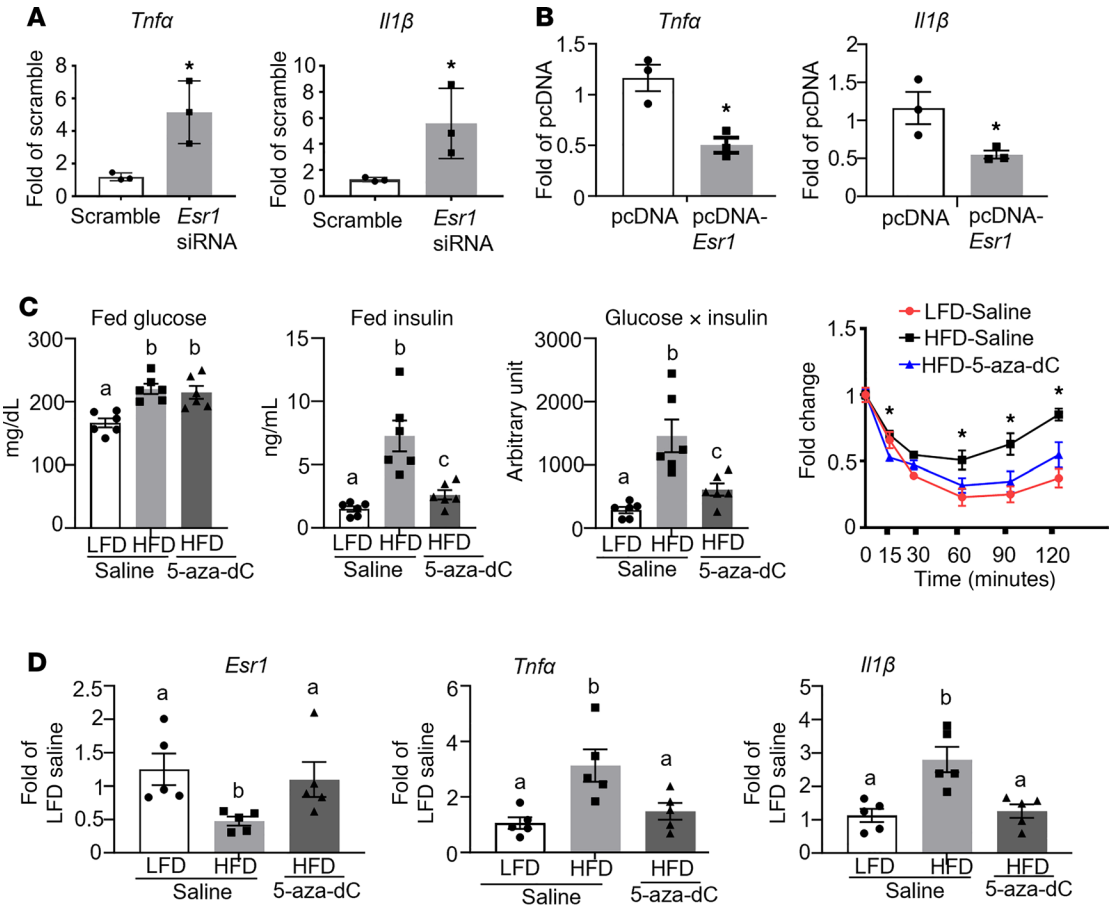


**Figure 3. Inhibiting DNA methylation increases *Esr1* expression and decreases inflammation in adipocytes.** (**A** and **B**) Pro-inflammatory gene expression in 3T3-L1 adipocytes with *Esr1* knockdown (**A**) or overexpression (**B**), $n$ = 3/group. *$P$ < 0.05 vs. Scramble in **A** or pcDNA in **B** by Student's $t$ test. (**C**) Plasma glucose, insulin, glucose × insulin products, and insulin tolerance test (ITT) in DIO mice treated with 5-aza-dC (0.25 mg/kg BW, 3 times per week) for 6 weeks, $n$ = 4–6/group. Groups labeled with different letters are statistically different from each other; *$P$ < 0.05 vs. other groups. Statistical significance was analyzed by 1-way ANOVA with Fisher's LSD post hoc test. (**D**) *Esr1* and pro-inflammatory gene expression in gWAT of DIO mice treated with 5-aza-dC (0.25 mg/kg BW, 3 times per week) for 6 weeks, $n$ = 5/group. Groups labeled with different letters are statistically different from each other as analyzed by Kruskal-Wallis nonparametric ANOVA by rank for *Esr1* and ANOVA with Fisher's LSD post hoc test for *Tnfα* and *Il1β*. All data are expressed as mean ± SEM.

To further study whether adipose tissue thermogenesis contributes to increased energy expenditure in female AD1KO mice, we measured thermogenic gene expression in brown and white adipose tissues of female AD1KO and fl/fl mice. As shown in Figure 5G, the expression of thermogenic genes, including uncoupling protein 1 (*Ucp1*), peroxisome proliferative activated receptor γ coactivator 1α (*Pgc1α*), *Pgc1β*, ELOVL fatty acid elongase 3 (*Elovl3*), cell death-inducing DNA fragmentation factor, α subunit-like effector A (*Cidea*), and epithelial V-like antigen 1 (*Eva1*) was upregulated in interscapular brown adipose tissue (iBAT). In consistency, IHC staining with anti-UCP1 antibodies also demonstrated increased UCP1 levels in iBAT of AD1KO mice (Figure 5H). In addition, the expression of several thermogenic genes and beige adipocyte markers, including *Pgc1α*; PR domain containing 16 (*Prdm16*); type 2 deiodinase (*Dio2*); cytochrome *c* oxidase subunit I (*Cox1*); acyl-Coenzyme A oxidase 1 (*Acox1*); kelch-like 13 (*Klhl13*); eosinophil-associated, ribonuclease A family, member 2 (*Ear2*); and T-box 1 (*Tbx1*), were also upregulated in gWAT of AD1KO mice (Figure 5I). These data suggest that adipocyte *Dnmt1* deletion promotes brown and beige adipocyte thermogenesis, which in turn contributes to increased energy expenditure observed in AD1KO mice.

Since *Dnmt1* deficiency suppresses adipocyte inflammation as shown above, we next examined adipose tissue inflammation in female AD1KO mice. *Dnmt1* deletion markedly decreased methylation rates on the individual CpG sites at the *Esr1* promoter as measured by pyrosequencing (Figure 6A). As expected, this was associated with an upregulation of *Esr1* expression and a reciprocal downregulation of inflammatory gene expression in gWAT of female AD1KO mice (Figure 6, B–F).

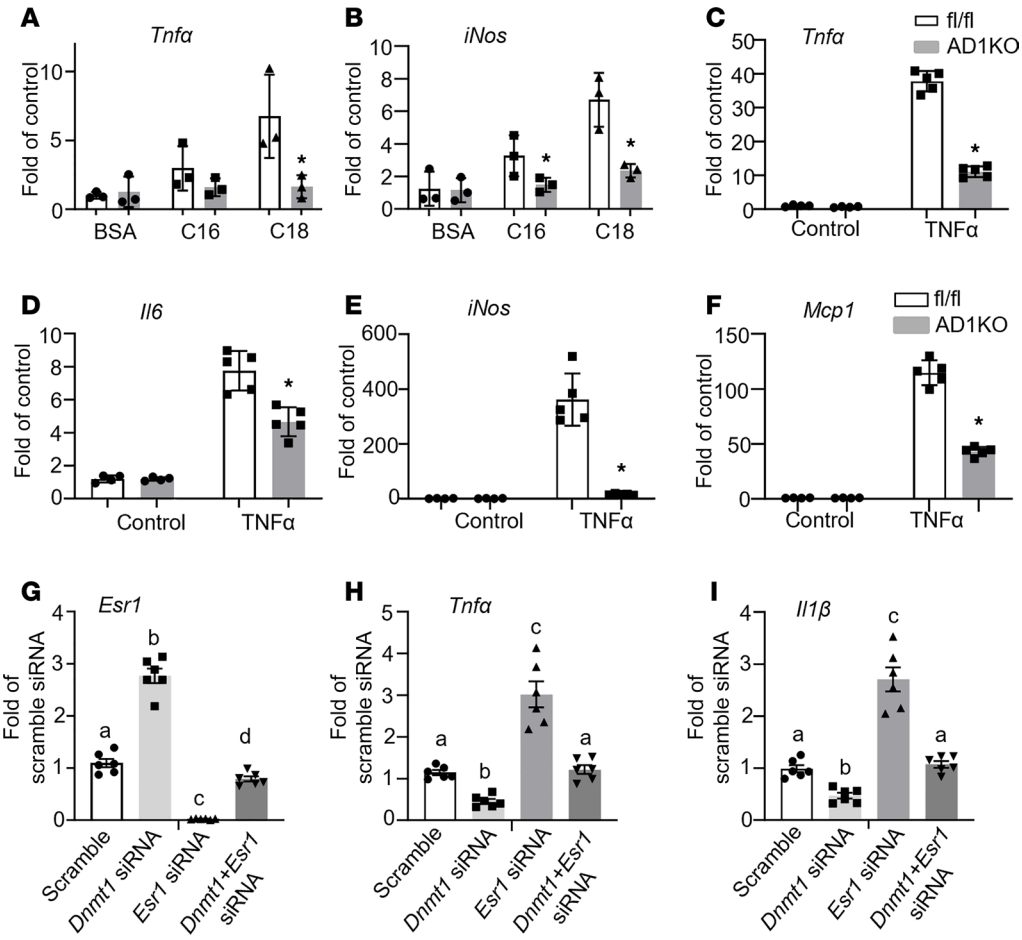


**Figure 4. Adipocyte *Esr1* mediates the beneficial effects of inhibiting DNA methylation–induced decrease in adipocyte inflammation.** (**A** and **B**) Pro-inflammatory gene *Tnfα* (**A**) and *iNos* (**B**) expression in adipocytes differentiated from AD1KO and fl/fl mice and treated with palmitate (C16) or stearate (C18), $n$ = 3/group. *$P$ < 0.05 vs. fl/fl by Student's $t$ test. (**C**–**F**) Pro-inflammatory gene *Tnfα* (**C**), *Il6* (**D**), *iNos* (**E**), and *Mcp1* (**F**) expression in adipocytes differentiated from AD1KO and fl/fl mice and treated with TNF-α, $n$ = 4–5/group. *$P$ < 0.05 vs. fl/fl by Student's $t$ test. (**G**–**I**) *Esr1* (**G**), *Tnfα* (**H**), and *Il1β* (**I**) expression in 3T3-L1 adipocytes with *Dnmt1* and/or *Esr1* knockdown. Day 5 differentiated 3T3-L1 cells were transfected with scramble, *Dnmt1*, *Esr1*, or both *Dnmt1* and *Esr1* siRNA. Two days later, cells were treated with TNF-α, and samples were collected for gene expression analysis. $n$ = 6. Groups labeled with different letters are statistically different from each other as analyzed by 1-way ANOVA with Fisher's LSD post hoc test. All data are expressed as mean ± SEM.

We further conducted RNA-Seq analysis in gWAT in female AD1KO and their fl/fl littermate mice to thoroughly characterize inflammatory status through gene expression profiling. The volcano plot revealed a downregulation of a panel of inflammatory/chemotactic genes in female *Dnmt1*-deficient gWAT (Figure 7A). This was consistent with the KEGG pathway analysis showing cytokine-cytokine receptor interaction, chemokine signaling pathway, and NF-κB signaling pathway among top ranked pathways identified (Figure 7B). Indeed, a hierarchical cluster analysis revealed a broad downregulation of chemotactic (e.g., chemokine [CC motif] ligand 2 [*Ccl2*/*Mcp1*], *Ccl3*, *Ccl4*) and pro-inflammatory genes (e.g., *Tnfα*, *Il1β*, *Nos2*/*iNos*) in gWAT of female AD1KO mice on HFD (Figure 7C).

We further assessed the status of macrophage infiltration into adipose tissue in female AD1KO mice. Histochemical staining with antibodies against macrophage marker CD68 revealed a substantial decrease of adipose tissue macrophage (ATM) content in gWAT of female AD1KO mice compared with that of fl/fl mice (Figure 8A). This was further verified by FACS analysis, which showed a significant reduction of $F4/80^+$ ATMs, $F4/80^+CD11C^+$ double-positive ATMs, and $CD8^+$ T lymphocytes, as well as a tendency of decreased $B220^+$ B lymphocytes in adipose tissue stromal vascular fraction cells in gWAT of female AD1KO mice compared with that of fl/fl mice (Figure 8, B and C). These data suggest that adipocyte *Dnmt1* deletion reduces macrophage and lymphocyte infiltration in adipose tissue, thereby suppressing adipose inflammation.

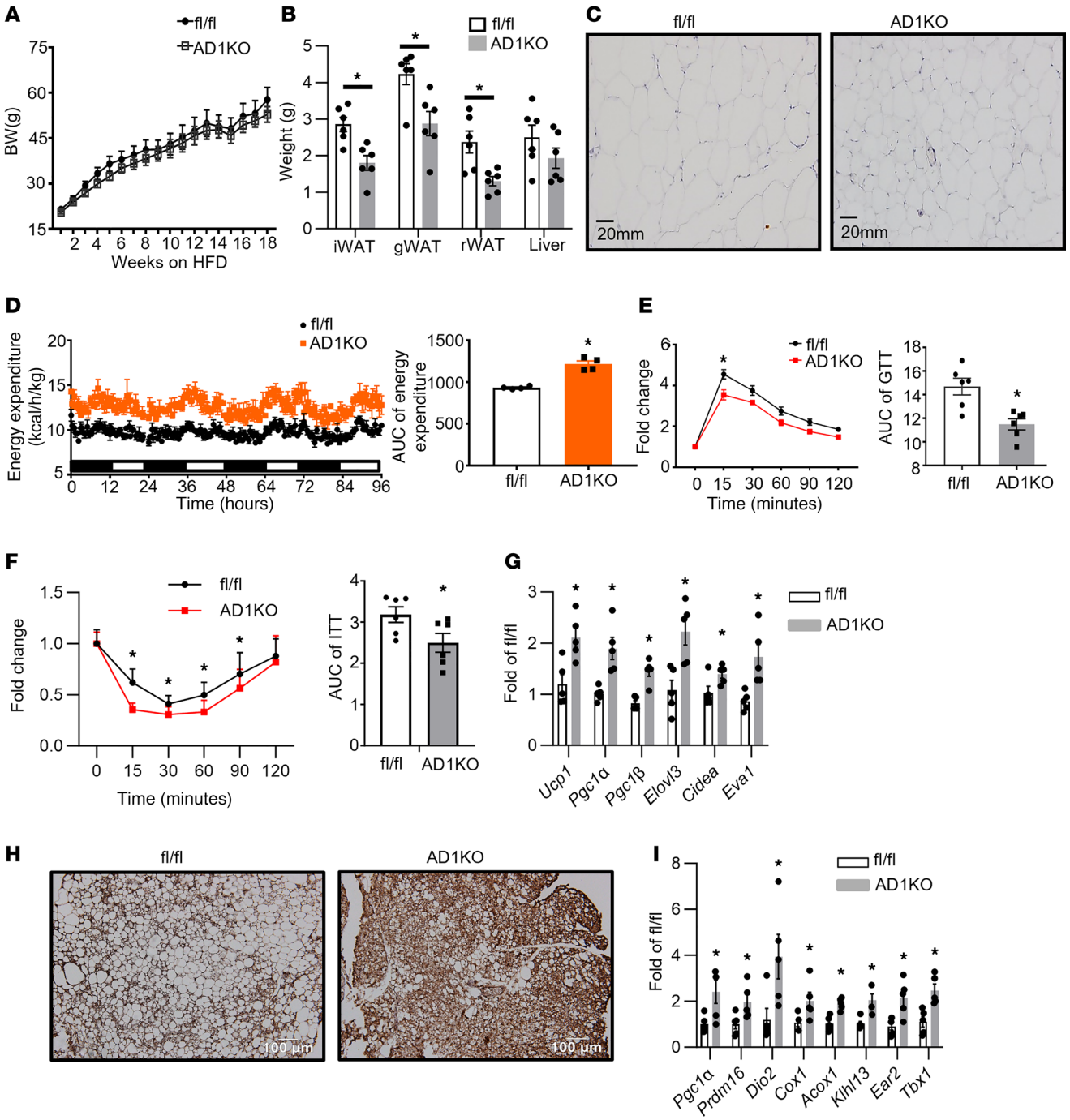


**Figure 5. Adipocyte *Dnmt1* deletion improves metabolic phenotypes in female mice fed HFD.** (**A** and **B**) Body weight (**A**) and adipose tissue and liver weight (**B**) in female AD1KO and fl/fl mice fed HFD, $n = 6$/group. *$P < 0.05$ vs. fl/fl by Student's $t$ test. (**C**) H&E staining of gWAT of female AD1KO and fl/fl mice fed HFD. Images are representative from 3 replicate samples. (**D**) Energy expenditure in female AD1KO and fl/fl mice fed HFD, $n = 4$/group. *$P < 0.05$ vs. fl/fl by Student's $t$ test. (**E** and **F**) Glucose tolerance test (GTT) (**E**) and ITT (**F**) in female AD1KO and fl/fl mice fed HFD, $n = 6$/group. *$P < 0.05$ vs. fl/fl by 1-way ANOVA with repeated measures followed by Fisher's LSD post hoc test. (**G**) Thermogenic expression in iBAT of female AD1KO and fl/fl mice fed HFD. $n = 5$. *$P < 0.05$ vs. fl/fl by Student's $t$ test. (**H**) UCP1 immunostaining in iBAT of female AD1KO and fl/fl mice on HFD. Images are representative from 3 replicate samples. (**I**) Thermogenic expression in gWAT of female AD1KO and fl/fl mice fed HFD. $n = 5$. *$P < 0.05$ vs. fl/fl by Student's $t$ test. All data are expressed as mean ± SEM.

We also characterized metabolic phenotypes of male AD1KO mice. There was no difference in body weight (Supplemental Figure 7A) and fat mass (Supplemental Figure 7B) between male AD1KO mice and their littermate control fl/fl mice. However, male AD1KO mice displayed a slight improvement in GTT (Supplemental Figure 7C). Quantitative PCR analysis also showed a slight decrease in the expression of *Il6* (Supplemental Figure 7D).

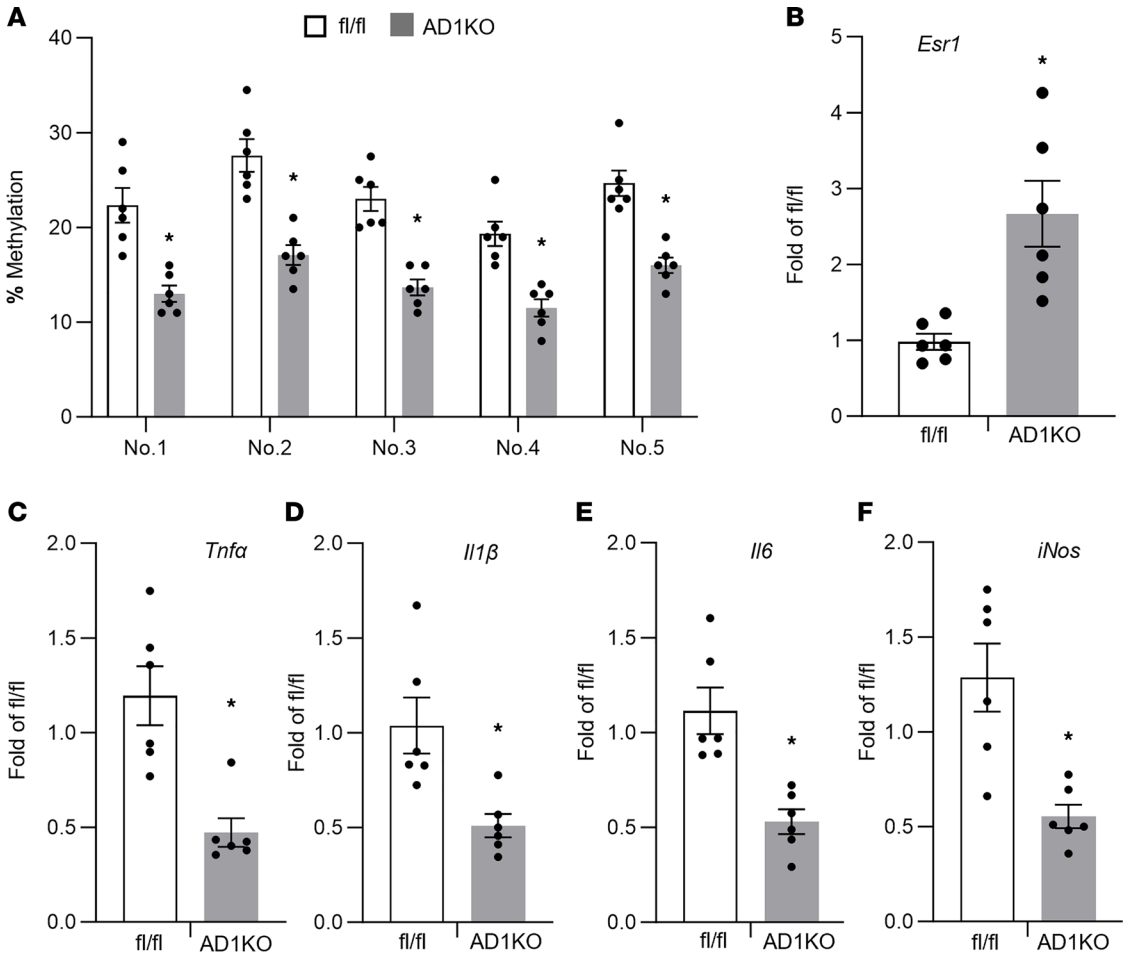


**Figure 6. Adipocyte *Dnmt1* deletion upregulates *Esr1* expression and reduces adipose tissue inflammation in female mice fed HFD.** (**A**–**F**) *Esr1* promoter DNA methylation level (**A**) and mRNA expression level, including *Esr1* (**B**), *Tnfα* (**C**), *Il1β* (**D**), *Il6* (**E**), and *iNos* (**F**) in female AD1KO and fl/fl mice fed HFD, $n = 6$/group. $^*P < 0.05$ vs. fl/fl by Student's *t* test. All data are expressed as mean ± SEM.

We generated AD3aKO mice by crossing *Dnmt3a*-floxed mice (20) with adiponectin-Cre mice (18) and observed around 75% reduction of *Dnmt3a* expression in gWAT of AD3aKO mice (Supplemental Figure 8A). HFD-fed female AD3aKO mice did not show differences in body weight, fat pad weight, glucose tolerance/insulin sensitivity, *Esr1* expression, and inflammatory gene expression in WAT (Supplemental Figure 8, B–E). There was also no difference in body weight between HFD-fed male AD3aKO and fl/fl mice (Supplemental Figure 9A). However, HFD-fed male AD3aKO mice had slightly improved glucose tolerance and insulin sensitivity (Supplemental Figure 9, B and C), with no changes in the expression of *Esr1* and inflammatory genes in gWAT (Supplemental Figure 9D).

*Targeted methylation at the Esr1 promoter regulates adipocyte inflammation/chemotaxis and insulin sensitivity*. Our data thus far suggest a key role of DNMT1 in the regulation of adipocyte inflammation and insulin sensitivity; however, it is not clear whether specific methylation at the *Esr1* promoter mediates the effect of DNMT1 in these processes. In addition, DNMT1 may have many downstream targets that confound the metabolic phenotypes observed in AD1KO mice. We therefore employed a modified CRISPR/RNA-guided system (21, 22) to specifically induce methylation/demethylation at the *Esr1* promoter. We first tested several single guide RNAs (sgRNAs) that surround the CpG sites at the *Esr1* promoter. We infected 3T3-L1 adipocytes with lentivirus expressing sgRNAs (Scramble or *Esr1* targeting) and dCas9-DNMT3a or dCas9-TET1 with *Esr1* mRNA as the readout. We identified 1 sgRNA (S7) that mediated the most potent inhibition or stimulation of *Esr1* expression for dCas9-DNMT3a and adCas9-TET1, respectively (Supplemental Figure 10).

To mimic the physiological milieu of adipose tissue where ATMs are recruited to fat tissue and constantly interact with adipocytes in a paracrine fashion, we examined adipocyte chemotaxis by a macrophage migration assay. We employed a coculture system where RAW264.7 murine macrophages

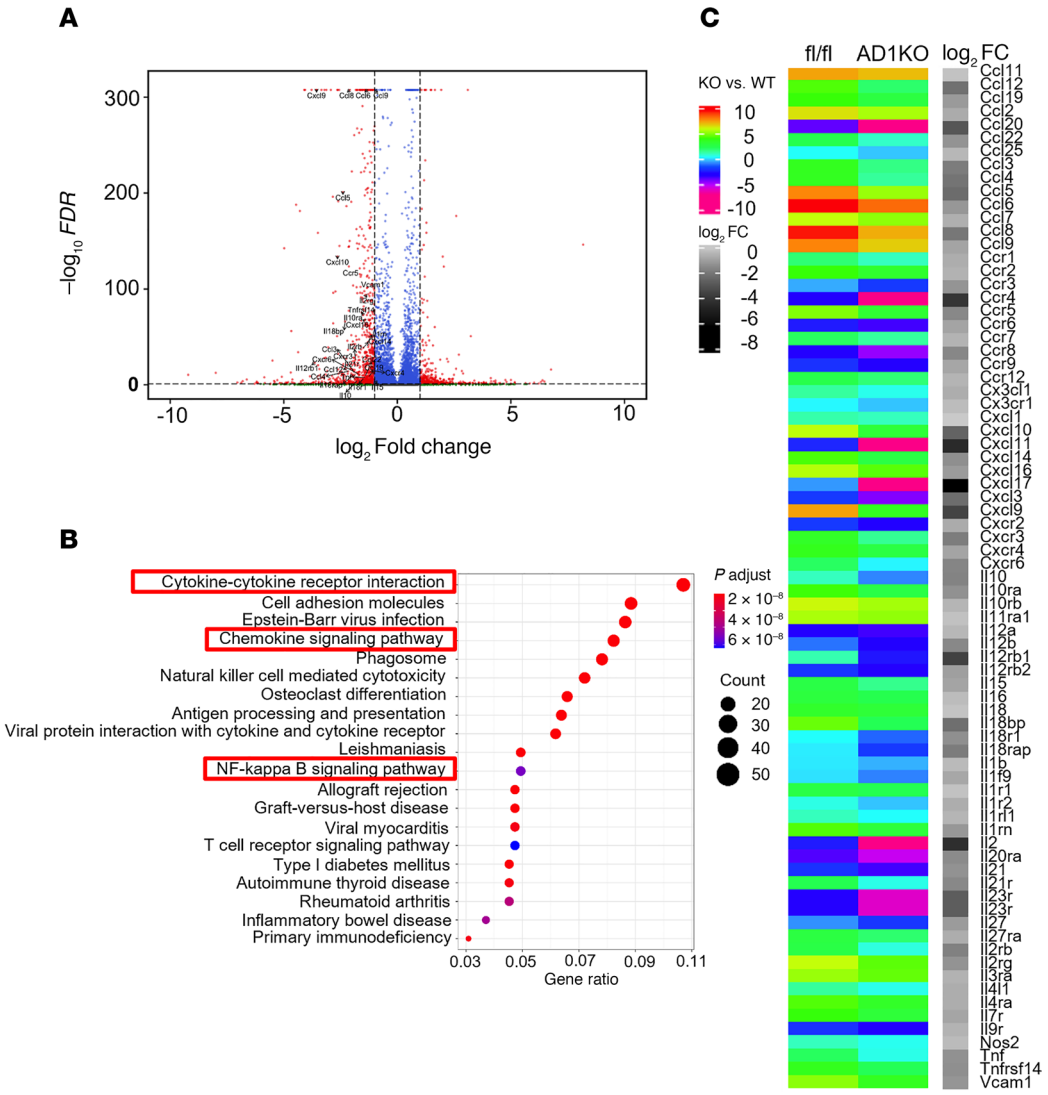


**Figure 7. RNA-Seq analysis in gWAT of female AD1KO and fl/fl mice fed with HFD.** (**A**–**C**) Volcano plot (**A**), pathway analysis (**B**), and heatmap (**C**) analyzed from RNA-Seq data from gWAT of female AD1KO and fl/fl mice fed with HFD. Equal amounts of RNAs from 4 animals/group were pooled and used for RNA-Seq analysis. RNA-Seq analysis was performed as described under Methods.

were grown in Transwell inserts, which were then placed into lower well chambers containing differentiated L1 adipocytes infected with lentivirus expressing dCas9-DNMT3a or dCas9-TET1 along with S7 sgRNA. We found more macrophage migration in Transwells cocultured with adipocytes infected with dCas9-DNMT3a and S7 sgRNA (Figure 9A). Meanwhile, the adipocytes infected with lentivirus expressing dCas9-DNMT3a and S7 sgRNA displayed enhanced pro-inflammatory gene expression over control adipocytes expressing scramble nontargeting sgRNA (Figure 9B). In contrast, we observed less macrophage migration in Transwells cocultured with adipocytes infected with dCas9-TET1 and S7 sgRNA (Figure 9C). The adipocytes expressing dCas9-TET1 and S7 sgRNA exhibited a significant decrease in pro-inflammatory gene expression (Figure 9D). These data suggest that DNA methylation at the *Esr1* promoter regulates adipocyte inflammation and chemotaxis.

To further investigate the role of DNA methylation at the *Esr1* promoter in the regulation of adipocyte inflammation and insulin sensitivity in vivo, we surgically injected lentivirus expressing dCas9-TET1 plus either the targeting S7 sgRNA or the scramble nontargeting sgRNA into gWAT of female C57BL6/J mice. Animals were then put on HFD for 12 weeks and were characterized for their metabolic phenotypes and adipose tissue inflammation. We successfully infected the fat depots with lentivirus expressing dCas9-TET1 as shown by mCherry IHC staining (Supplemental Figure 11A). Mice injected with lentivirus expressing

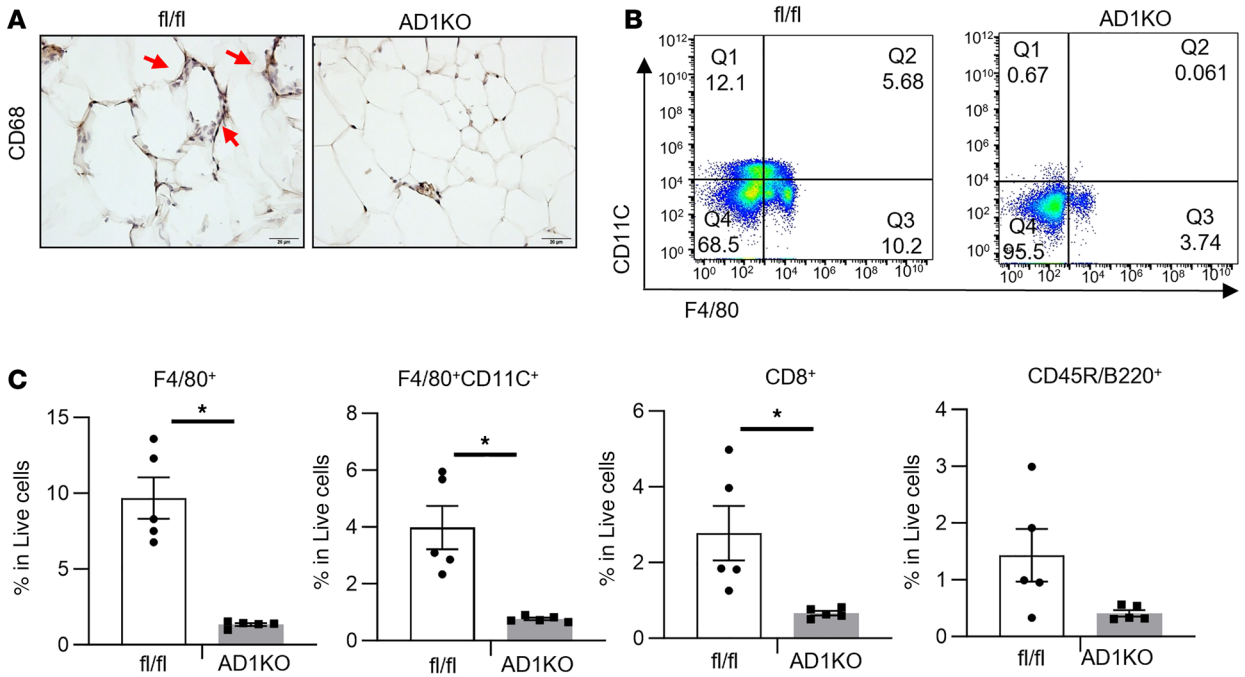


**Figure 8. Adipocyte-specific deletion of Dnmt1 results in reduced immune cell infiltration in gWAT of female AD1KO compared with that of fl/fl mice fed HFD.** (**A**) CD68 immunostaining of gWAT of female AD1KO and fl/fl mice fed HFD. Images are representative from 3 replicate samples. Scale bar, 20 μm. (**B**) FACS analysis of F4/80$^+$CD11C$^+$ ATMs in gWAT of female AD1KO and fl/fl mice fed HFD. Images are representative from 5 replicate samples. (**C**) Percentage of F4/80$^+$ ATMs, F4/80$^+$CD11C$^+$ ATMs, CD8$^+$ T lymphocytes, and CD45R/B220$^+$ B lymphocytes in gWAT of female AD1KO and fl/fl mice fed HFD, $n$ = 5/group. *$P$ < 0.05 vs. fl/fl by Student's $t$ test. All data are expressed as mean ± SEM.

dCas9-TET1 and S7 sgRNA had no difference in body weight (Supplemental Figure 11B); however, they exhibited improved glucose tolerance and insulin sensitivity as assessed by glucose and insulin tolerance tests compared with mice injected with lentivirus expressing dCas9-TET1 and scramble sgRNA (Figure 10, A and B). Moreover, lentiviral infection with dCas9-TET1 and S7 sgRNA increased *Esr1* gene expression in gWAT (Figure 10C). This was associated with decreased expression of inflammatory genes, such as *Tnfα* and *Il1β*, in gWAT (Figure 10C). FACS analysis also revealed a significant reduction of F4/80$^+$ ATMs, F4/80$^+$CD11C$^+$ double-positive ATMs, and CD8$^+$ T lymphocytes in gWAT of HFD-fed mice injected with lentivirus expressing dCas9-TET1 and S7 sgRNA (Figure 10, D and E).

## Discussion

In this study, we tested the hypothesis that epigenetic regulation at the *Esr1* promoter by HFD feeding, which often causes obesity, mediates adipocyte inflammation and chemotaxis, leading to obesity-induced insulin resistance and type 2 diabetes. The premise of this hypothesis stems from several prior observations. For one, chronic inflammation is a key link between obesity and insulin resistance/type 2 diabetes, and adipose tissue plays an important role in obesity-induced inflammation and insulin resistance (1, 2). Second, inflammatory signaling pathways in adipose tissue can be activated in nutrient-rich conditions (e.g., HFD feeding) (3). However, it is not fully understood how HFD feeding alters the inflammatory program. Our study demonstrates that enhanced DNA methylation at the *Esr1* promoter by HFD plays an important role in mediating exaggerated adipose chemotaxis and inflammation, which may contribute to obesity-induced insulin resistance and type 2 diabetes.

Estrogen receptors (ESRs or ERs), members of the nuclear receptor family, play a pivotal role in various metabolic and developmental processes, including metabolism, glucose homeostasis, differentiation, cell proliferation, and immune-regulatory and antiinflammatory function (14). There are 2 isoforms of ERs: ERα and ERβ, which are encoded by *Esr1* and *Esr2* genes, respectively (14). ERα (ESR1) is the predominant form in adipocytes (14). Evidence shows that ERα/ESR1 in the brain regulates food intake and energy metabolism (23). Mice with whole-body deficiency of *Esr1* develop insulin resistance, suggesting a protective role of *Esr1* in insulin sensitivity (24). In addition, *Esr1* has an antiinflammatory function in immune cells because of its ability to interfere with the NF-κB pathway (14). Recent studies have also demonstrated the antiinflammatory role of *Esr1* in adipocytes (14–16). Genetic ablation of *Esr1*

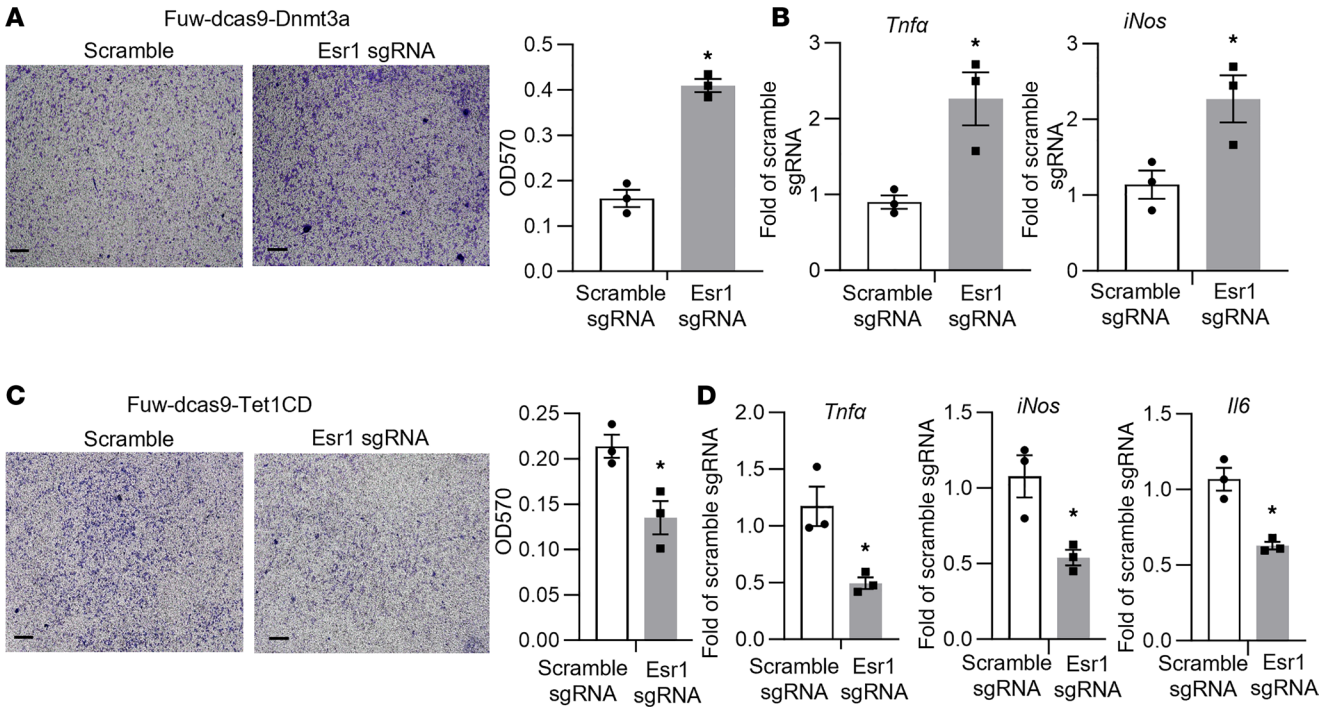


**Figure 9. Targeted methylation at the *Esr1* promoter in adipocytes regulates macrophage inflammation and chemotaxis in an adipocyte-macrophage coculture system.** (**A** and **B**) Macrophage migration assay (**A**) and inflammatory gene expression (**B**) in RAW264.7 macrophages cocultured with 3T3-L1 adipocytes infected with lentivirus expressing scramble sgRNA or S7 sgRNA targeting *Esr1* promoter along with dCas9-DNMT3a. *n* = 3/group, **P* < 0.05 vs. Scramble by Student's *t* test. Images in **A** are representative from 3 replicate samples. (**C** and **D**) Macrophage migration assay (**C**) and inflammatory gene expression (**D**) in RAW264.7 macrophages cocultured with 3T3-L1 adipocytes infected with lentivirus expressing scramble sgRNA or S7 sgRNA targeting *Esr1* promoter along with dCas9-TET1. *n* = 3/group, **P* < 0.05 vs. Scramble by Student's *t* test. Images in **C** are representative from 3 replicate samples. All data are expressed as mean ± SEM.

in adipocytes enhances adipose inflammation and macrophage infiltration, which might be mediated by increased *Mcp1* expression in adipocytes because of *Esr1* deficiency (15, 16). This may contribute to *Esr1*'s protective effect on insulin sensitivity (24). Here we discovered that HFD feeding significantly increased the binding of DNMT1 at the *Esr1* promoter, which resulted in increased DNA methylation at the *Esr1* promoter and subsequent downregulation of *Esr1* expression (Figure 2A). Indeed, we found *Dnmt1* deficiency in adipocytes increased *Esr1* expression, resulting in decreased adipocyte chemotaxis. AD1KO mice with *Dnmt1* deficiency in adipocytes displayed increased *Esr1* expression, decreased adipose inflammation, and improved insulin sensitivity upon HFD challenge. The antiinflammatory effect of *Dnmt1* deficiency can be attributed to the decreased DNA methylation at the *Esr1* promoter, because specifically reducing DNA methylation at the *Esr1* promoter using a modified CRISPR/RNA-guided system increased *Esr1* expression, decreased adipose inflammation, and improved insulin sensitivity in mice fed HFD, essentially recapitulating the phenotype of AD1KO mice.

Accumulating evidence suggests that epigenetic regulation plays a significant role in the development of obesity and its related disorders, such as type 2 diabetes (25–29). However, relatively few studies address the role of epigenetics, particularly DNA methylation, in obesity-induced inflammation. We recently reported that inhibiting DNA methylation pharmacologically by 5-aza-dC ameliorated atherosclerosis in low-density lipoprotein receptor–knockout ($Ldlr^{-/-}$) mice (30). This was associated with attenuated macrophage migration and adhesion to endothelial cells and reduced macrophage infiltration into atherosclerotic plaques (30). We also found that *Dnmt1* and *Dnmt3b* expressed in macrophages regulate macrophage polarization and inflammation, which further affects insulin sensitivity in vivo and in vitro (10, 31). Here we demonstrated a key role of adipocyte DNA methylation in mediating adipocyte chemotaxis and inflammation. Our data indicate that enhanced DNA methylation at the *Esr1* promoter by HFD suppresses *Esr1* expression in adipocytes, which may dampen its antichemotactic function and thus increase macrophage infiltration into adipose tissue. Meanwhile infiltrated macrophages in adipose tissue may undergo a phenotypic change toward a more pro-inflammatory spectrum via an epigenetic mechanism involving DNA methylation. Enhanced DNA methylation at the *Pparγ*

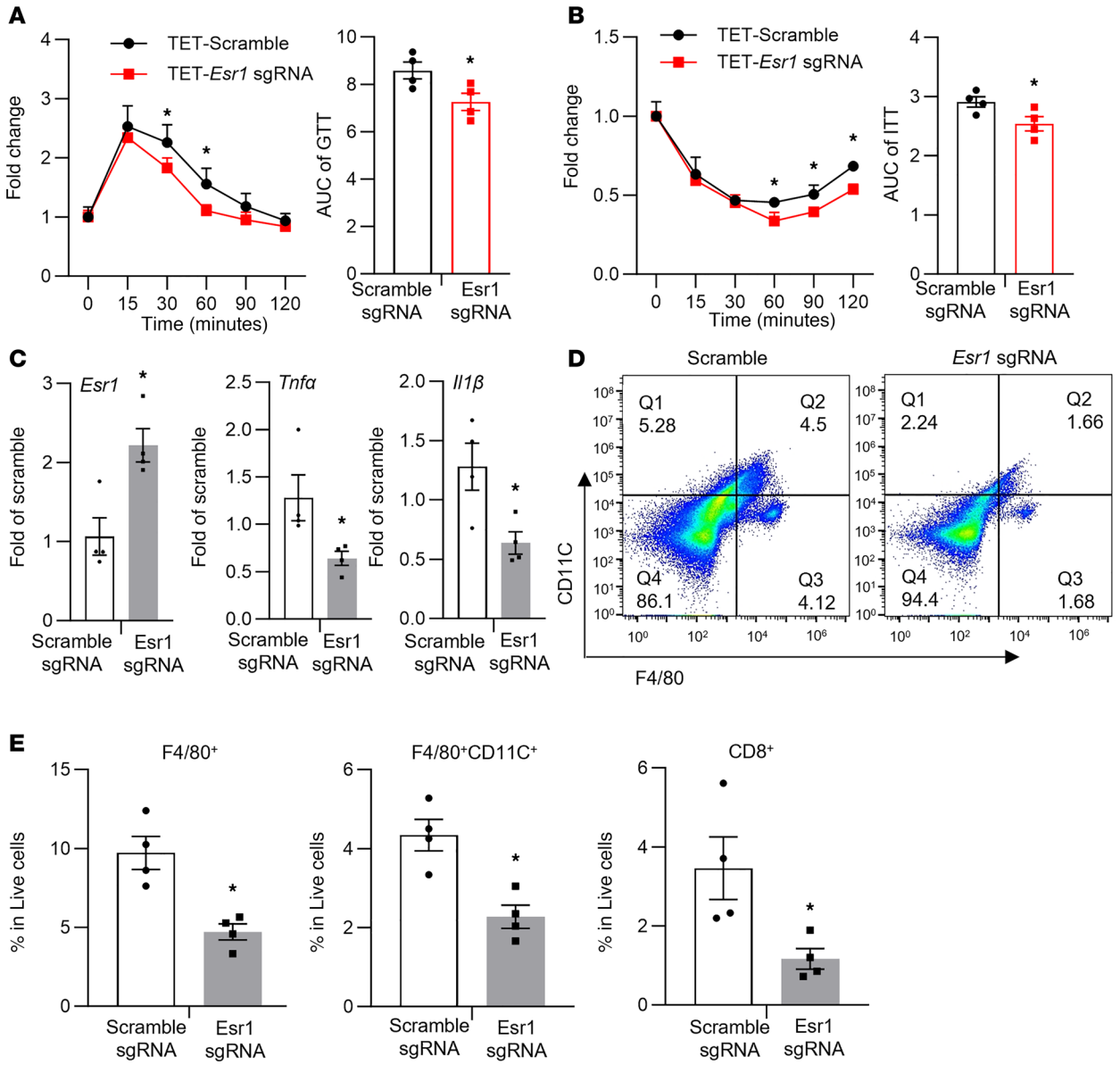


**Figure 10. Targeted methylation at the *Esr1* promoter regulates adipose tissue inflammation and insulin sensitivity.** (**A** and **B**) GTT (**A**) and ITT (**B**) in HFD-fed female C57BL/6J mice surgically injected with dCas9-TET1 along with either scramble sgRNA or S7 sgRNA targeting *Esr1* promoter in gWAT, $n = 4$. *$P < 0.05$ vs. Scramble sgRNA by 1-way ANOVA with repeated measures followed by Fisher's LSD post hoc test. (**C**–**E**) Gene expression (**C**), FACS analysis of F4/80$^+$CD11C$^+$ ATMs (**D**), and percentage of F4/80$^+$ ATMs, F4/80$^+$CD11C$^+$ ATMs, and CD8$^+$ T lymphocytes (**E**) in gWAT of HFD-fed female C57BL/6J mice surgically injected with dCas9-TET1 along with either scramble sgRNA or S7 sgRNA targeting *Esr1* promoter in gWAT, $n = 4$. *$P < 0.05$ vs. Scramble sgRNA by Student's *t* test. All data are expressed as mean ± SEM.

promoter by HFD decreases *Pparγ* expression in ATMs, promoting M1 macrophage polarization and inflammation (10, 31). It has been well documented that in the fat tissue, adipocytes and macrophages interact synergistically to generate inflammatory response and mediators in obesity (1, 32–35). Our study helps us further understand adipose tissue inflammation from the perspective of epigenetic regulation.

Although DNMT1 is traditionally viewed as a maintenance enzyme that maintains DNA methylation patterns in dividing cells, several lines of evidence have pointed to a role for Dnmt1 beyond just maintaining methylation (7, 36). DNMT1 may also be involved in participation of de novo methylation on double-stranded DNA via a synergistic action along with other DNA methyltransferases (7, 37, 38). Since adiponectin-Cre we used to delete DNMT1 in adipocytes is primarily expressed in mature adipocytes (39), it is likely that DNMT1 exerts its pro-inflammatory function primarily by participating in de novo DNA methylation processes in adipocytes.

It is noteworthy that female AD1KO mice on HFD exhibited a stronger phenotype in improved insulin sensitivity and adipose inflammation than male AD1KO mice. Although the reason is not clear, estrogen as the ERα/ESR1 ligand may play a role. The presence of estrogen may synergistically activate the enhanced expression of *Esr1* caused by *Dnmt1* deficiency, leading to a more potent antiinflammatory effect in adipocytes. Of note, while male AD1KO mice had little change in body weight, female AD1KO mice had a reduced adiposity upon HFD challenge, which may also contribute to their improved insulin sensitivity. The reduced adiposity in female AD1KO mice may be primarily due to their increased energy expenditure, as there was no change in food intake between HFD-challenged female AD1KO mice and fl/fl controls. Indeed, we found that HFD-challenged female AD1KO mice had significantly upregulated thermogenic markers in both brown and white adipose tissues, which could contribute to their increased energy expenditure. It is well documented that activation of ESR1 stimulates brown adipocyte thermogenesis and white adipocyte beiging (40, 41). Thus, we found that increased *Esr1* expression in adipocytes due to *Dnmt1* deficiency could in turn promote brown and beige adipocyte thermogenesis in AD1KO mice and contribute to their increased energy expenditure, reduced adiposity, and improved metabolic phenotypes.

Both brown and white adipose tissues are innervated by the sympathetic nervous system (SNS) that is important in regulating brown and beige adipocyte thermogenesis (42–45). Recent data suggest that adipose tissue–derived neurotrophic factors and their receptors, including nerve growth factor (NGF) and its receptor tropomyosin receptor kinase A (TRKA) (46), brain-derived neurotrophic factor (BDNF) and its receptor tropomyosin receptor kinase B (TRKB) (47), and neurotrophic factor 3 (NT3) and its receptor tropomyosin receptor kinase C (TRKC) (48), are important in regulating SNS innervation in adipose tissue. Interestingly, it has been shown that estrogen and its receptor ESR1 promotes neuronal growth and development through interactions with the neurotrophins and their receptors (49), and estrogen stimulates the expression and production of these neurotrophic factors, including NGF, BDNF, and NT3, in various brain regions and peripheral tissues (50–54). Thus, it is possible that promoting sympathetic nerve innervation in adipose tissue by estrogen and ESR1 via neurotrophic factor production may be another mechanism mediating ESR1's effects on brown/beige adipocyte thermogenesis in AD1KO mice. Interestingly, during the conduct of our study, a recent report indicated that adipocyte DNMT3a mediates obesity-induced insulin resistance via increasing DNA methylation at the *Fgf21* gene (55). Taken together, DNA methylation catalyzed by DNMT1 and -3a may regulate adipocyte energy metabolism and inflammation via various pathways.

While our studies on the adipocyte DNMT1 are still ongoing, a recent study by Park et al. showed the opposite metabolic phenotype using a similar adipocyte-specific DNMT1-deficient mouse line (56). In the study by Park et al., adipocyte-specific DNMT1-deficient mice gained significantly more weight even on a normal chow diet and were further prone to diet-induced obesity when fed an HFD (56); whereas in our hands, our AD1KO mice had lower adiposity when fed an HFD, albeit with no changes in body weight. Although the exact reason for this discrepancy is not clear, several differences between the two studies may contribute to the different metabolic phenotypes observed. First, in the study by Park et al., metabolic studies were performed from only male mice, whereas in our study, we used both male and female AD1KO and fl/fl control mice. We did not find much metabolic difference between male AD1KO and fl/fl mice; thus, our study has primarily focused on female AD1KO mice. Second, there are several DNMT1-floxed mouse lines as well as adiponectin-Cre lines available according to Mouse Genome Informatics (MGI) (https://www.informatics.jax.org/allele/summary?markerId=MGI:94912, https://www.informatics.jax.org/allele/summary?markerId=MGI:106675). We obtained DNMT1-floxed mice from Mutant Mouse Regional Resource Centers (MMRRC) (*Dnmt1*-floxed line: MMRRC No. 014114) (17), which was created by inserting 2 *loxP* sites flanking exons 4 and 5, causing a frame shift and lacking the motifs for the catalytic domain. For the adiponectin-Cre line, we obtained it from Jackson Laboratory (Stock 010803) (18), in which a BAC transgene was used to express Cre-recombinase under the control of adiponectin promoter. However, there was no information from Park et al. regarding either the DNMT1-floxed mouse line or adiponectin-Cre line used in the study. It is possible that different DNMT1-floxed mouse lines and/or adiponectin-Cre lines used in the 2 studies may contribute to the discrepancy in mouse metabolic phenotypes observed. Third, differences in the genetic background of animals used in the two studies, or differences in diet and animal housing facilities, may also contribute to the differences in the metabolic phenotypes observed in the two studies. Thus, further study is warranted to clarify the role of adipocyte DNMT1 in the regulation of adipocyte metabolic function.

In summary, we discovered that HFD feeding significantly enhanced DNA methylation at *Esr1* promoter in adipocytes, which is associated with downregulation of *Esr1* expression. *Dnmt1* deletion in adipocytes increased *Esr1* expression, decreased adipose inflammation, and improved insulin sensitivity in female mice with HFD challenge. Specifically reducing DNA methylation at the *Esr1* promoter using a CRISPR/RNA-guided system can largely recapitulate the phenotypes of adipocyte *Dnmt1*-deficient mice, suggesting a key role of DNA methylation at the *Esr1* promoter in regulating adipocyte chemotaxis and adipose inflammation. Deregulated epigenetic regulation, presumably by HFD, may result in altered adipocyte inflammation and chemotaxis, thereby contributing to obesity-induced inflammation and insulin resistance.

## Methods

*Sex as a biological variable*. Our study examined both male and female mice. Results from both male and female mice were reported.

*Mice*. Mice with adipocyte-specific *Dnmt1* or *Dnmt3a* knockout (AD1KO or D3aKO) were generated by crossing *Dnmt1*- or *-3a*-floxed mice (obtained from MMRRC; *Dnmt1*-floxed line: MMRRC No. 014114; *Dnmt3a*-floxed line: MMRRC No. 029885) with adiponectin-Cre mice (Jackson Laboratory, Stock No. 010803) (18). The *Dnmt1*-floxed mouse was created by inserting 2 *loxP* sites flanking exons 4 and 5, which causes frameshift and lack of the motifs for the catalytic domain (17). The *Dnmt3a*-floxed mouse was created by inserting 2 *loxP* sites flanking exon 19, which encodes the catalytic motif (20). For 5-aza-dC treatment study, 6-week-old male C57BL/6J mice were fed either an LFD (Research Diets D12450B, 10% calories from fat) or an HFD (Research Diets D12492, 60% calories from fat) for 16 weeks to establish diet-induced obesity and were then randomly assigned to receive either saline or 5-aza-dC (0.25 mg/kg) injection i.p. 3 times per week for up to 6 weeks. All the mice were housed in a temperature- and humidity-controlled animal research facility with a 12/12 hours light/dark cycle and having ad libitum access to food and water.

*Metabolic measurement*. AD1KO and D3aKO mice and their respective floxed controls (fl/fl) were fed either LFD (Research Diets D12450B, 10% calorie from fat) or HFD (Research Diets D12492, 60% calorie from fat) for up to 20 weeks. The following metabolic measurements were conducted. 1) Body weight was measured weekly, and food intake of singly housed mice was measured over 7 consecutive days. 2) Blood glucose levels were measured by OneTouch Ultra Glucose meter (LifeScan). GTT and ITT were conducted to determine glucose tolerance and insulin sensitivity as we previously described (10). 3) Energy expenditure was measured using PhenoMaster metabolic cage systems (TSE Systems). At the end of HFD-feeding studies, various white fat depots were dissected for further assessment of inflammatory status, including inflammatory gene expression, IHC, and FACS analysis as described below.

*RNA extraction and quantitative reverse transcription PCR*. Total RNA from fat tissues or cultured adipocytes was isolated using the Tri Reagent kit (Molecular Research Center). The mRNA levels of the genes of interest were quantitated by a 1-step quantitative reverse transcription PCR with a TaqMan Universal PCR Master Mix kit (Thermo Fisher Scientific) using an Applied Biosystems QuantStudio 3 real-time PCR system (Thermo Fisher Scientific) as we previously described (10). The TaqMan primers/probes for all the genes measured were either purchased from Applied Biosystems (Thermo Fisher Scientific) or commercially synthesized (Supplemental Table 1).

*Immunoblotting*. Protein abundance in tissues was measured by immunoblotting as we described (10). Adipose tissue was homogenized in a modified RIPA lysis buffer supplemented with 1% protease inhibitor mixture and 1% phosphatase inhibitor mixture (Sigma-Aldrich). Lysates were resolved by SDS-PAGE gels and were transferred to nitrocellulose membranes (Bio-Rad), which underwent blocking, washing, and sequential incubation with various primary antibodies and Alexa Fluor 680–conjugated secondary antibodies (Life Science Technologies). The blots were developed with the LI-COR Imager System (LI-COR Biosciences). The antibodies were listed in Supplemental Table 2.

*IHC*. gWAT was fixed in 10% neutral formalin, embedded in paraffin, and sectioned at 5 μm thickness. The sections were immunostained with the primary and secondary antibodies, which were then developed with a peroxidase substrate from the DAB peroxidase substrate kit (Vector Labs, SK-4100). The primary and secondary antibodies are listed in Supplemental Table 2.

*Cell culture and siRNA knockdown*. 3T3-L1 preadipocytes (ATCC, Cl-173) were cultured in a DMEM growth medium and were induced to differentiate into mature adipocytes with a differentiation cocktail as we previously described (57). Primary preadipocytes isolated from mouse gonadal white fat were cultured and differentiated as previously described (10). For siRNA knockdown assays, day 5 or day 8 adipocytes were electroporated with

targeting siRNA or nontargeting scramble siRNA (GE Healthcare, now Cytiva) using Amaxa Nucleofector II Electroporator (Lonza) with an Amaxa cell line nucleofector kit L (Lonza) as we previously described (58, 59), and cells were harvested 2–3 days after the transfection for further analysis.

*FACS analysis*. FACS analysis of the macrophage content in adipose tissue was conducted as we previously described (10). Briefly, stromal vascular fraction cells were isolated from epididymal fat using collagenase digestion, Cells were sequentially incubated with FcBlock (eBioscience) and APC-F4/80 (clone A3-1, AbD Serotec), PE-Cy7-CD11c (clone HL3, BD Pharmingen), APC-Cy7-CD8 (clone 53-6.7, BD Pharmingen), and Pacific blue-B220 (clone RA3-6B2, BD Pharmingen), followed by washing with the FACS buffer, fixing with paraformaldehyde, and analyzing with BD FACSCalibur.

*Adipocyte chemotaxis*. Adipocyte chemotaxis was assessed by a macrophage migration assay as we previously described (30, 60). Briefly, we employed an adipocyte-macrophage coculture system where RAW264.7 macrophages (ATCC TIB-71) were grown in Transwell inserts, which were then placed into lower well chambers containing differentiated 3T3-L1 adipocytes with *Dnmt1* knockdown. Migrated cells were dissociated from the membrane, lysed, and quantified using CyQuant GR fluorescent dye with a Victor 3 plate reader (PerkinElmer).

*Esr1 promoter cloning and luciferase reporter assays*. A 1 kb fragment covering the *Esr1* proximal promoter and the 5′-UTRs enriched with CpG sites was PCR-implied from mouse genomic DNA with primers listed in Supplemental Table 3. The PCR fragment was further subcloned into pGL3 basic luciferase reporter (Promega). The test to compare the activity of fully methylated versus unmethylated Esr1 promoter was conducted as we previously described (10). The unmethylated promoter reporter was obtained by transforming the construct into *dam*$^-$/*dcm*$^-$ *E. coli* strain (New England Biolabs), while the fully methylated reporter was obtained by treating the construct with *SssI* methylase (New England Biolabs) in the presence of *S*-adenosylmethionine. The unmethylated or methylated *Esr1* reporter constructs were transfected into 3T3-L1 cells for luciferase activity measurement as we previously described (10).

*RRBS*. The whole-genome DNA methylation was assessed using RRBS (11–13). Briefly, genomic DNA from the mouse epididymal white fat was extracted by the phenol-chloroform method and commercially sequenced by Beijing Genomics Institute (BGI) (Shenzhen, China). According to the instructions provided by the company, the genomic DNA was digested with the methylation-insensitive restriction enzyme *MspI*, ligated to sequencing adaptors, treated with sodium bisulfite, PCR-amplified for library construction, and sequenced. The RRBS data analysis including DMRs, methylation rate, and pathway analysis were conducted by BGI Bioinformatics Center or using the bioinformatics analysis pipeline as described before (61). The methylation level at each CpG site was determined based on the number of sequences containing methylated CpGs versus the total number of sequences analyzed. For the comparison of DNA methylation rate differences between the HFD- and LFD-fed mice, data were summarized based on genomic features to generate tag density plots around transcription start and termination sites, exon-intron boundaries, CpG islands, and repeat elements, and the data were uploaded to UCSC Genome Browser on Mouse (NCBI37/mm9) Assembly for methylated gene mapping as reported previously (61). GO and KEGG pathway analyses were performed with R package (v.3.2.0).

*RNA-Seq analysis*. Total RNA was isolated from gWAT as described above and was submitted to BGI for RNA-Seq analysis. Equal amounts of RNAs from 4 animals/group were pooled and used for RNA-Seq analysis. Clean reads were aligned to the mouse reference genome (UCSC mm9). Differentially expressed genes between groups were defined as Log2 fold change ≥ 0.5 or ≤ –0.5. GO and KEGG pathway analysis were performed with R package (v.3.2.0).

*ChIP assays*. ChIP assay was used to assess the binding of DNMTs to the *Esr1* promoter as we previously described (58). Fat tissue was fixed to isolate nuclei, which were sonicated to shear DNA. The DNA was immunoprecipitated with DNMT1 or DNMT3a antibodies, eluted, and followed by quantitative PCR using SYBR green. Primer sequences used in this study were shown in Supplemental Table 4.

*Bisulfite conversion and pyrosequencing*. Pyrosequencing analysis was conducted to assess DNA methylation levels at *Esr1* promoter as we previously described (10). The genomic DNA from fat tissue was extracted by phenol/chloroform and followed by bisulfite conversion with an EpiTech Bisulfite Kit (QIAGEN). The bisulfite-converted DNA was PCR-amplified, and the pyrosequencing was carried out by EpiGenDx. The pyrosequencing primers for the *Esr1* promoter are shown in Supplemental Table 5.

*Targeted DNA methylation at the Esr1 promoter*. The mammalian lentiviral vectors FUW carrying dCas9-DNMT3a or dCas9-TET1, in which the catalytically inactive Cas9 (dCas9) has been engineered to be fused with the DNMT3a or TET1 (21, 22), were purchased from Addgene (Addgene No. 84476 and 84475).

The guide RNA sequences targeting the CpG sites at the *Esr1* promoter was designed with GT-Scan website (https://gt-scan.csiro.au), and the targeting or nontargeting oligos were synthesized, annealed, and subcloned into the *AarI* sites of the pgRNA lentiviral vector (Addgene no. 44248). Lentivirus expressing dCas9-TET1-CD, dCas9-DNMT3a, or sgRNA was commercially produced by Vigene Biosciences, Inc., and 10 μL of lentivirus ($1 \times 10^5$ transduction units/μL of titer) was surgically injected into mouse gonadal fat depots. Detailed primer information is listed in Supplemental Table 6.

*Statistics*. Student's 2-tailed *t* test, 1-way or 2-way ANOVA with Fisher's LSD post hoc test, or Kruskal-Wallis nonparametric ANOVA by rank was performed to evaluate statistical significance using GraphPad Prism version 5.0. In some experiments, 1-way or 2-way ANOVA with repeated measures was used for statistical analysis. Statistical significance was considered at $P < 0.05$. All data are shown as mean ± SEM.

*Study approval*. All animal procedures conducted in the study were approved by the IACUC at Georgia State University.

*Data availability*. The RNA-Seq and RRBS data have been deposited to National Center for Biotechnology Information Gene Expression Omnibus database with the accession number GSE301006. Values for graphs in the figures and supplemental figures are provided in the Supporting Data Values file.

## Author contributions

RW performed experiments and data analysis; FL, SW, JJ, and XC assisted in experiments and data collection; Huidong Shi, XC, SW, YH, XZ, JAC, ZD, and JS assisted in RRBS and RNA-Seq data analysis; LY contributed to study design, contributed conceptual and technical inputs, and reviewed and edited the manuscript; and BX and Hang Shi designed the study and wrote the manuscript.

## Acknowledgments

This work was supported in part by NIH grants R01DK118106 and R01DK125081 to BX; NIH grants R01DK115740, R01DK118106, R01DK116806, and R01DK130342 to HS; and NIH grants R01DK116496, R01DK111052, and R01DK130342 to LY. This work is the result of NIH funding, in whole or in part, and is subject to the NIH Public Access Policy. Through acceptance of this federal funding, the NIH has been given a right to make the work publicly available in PubMed Central.

Address correspondence to: Hang Shi or Bingzhong Xue, Department of Biology, Georgia State University, PO Box 4010, Atlanta, Georgia 30302, USA. Phone: 404.413.5799; Email: hshi3@gsu.edu (HS). Phone: 404.413.5747; Email: bxue@gsu.edu (BX).
JAC's present address is: Council on Dairy Cattle Breeding, Bowie, Maryland, USA.

1. Hotamisligil GS. Inflammation and metabolic disorders. *Nature*. 2006;444(7121):860–867.
2. Olefsky JM, Glass CK. Macrophages, inflammation, and insulin resistance. *Annu Rev Physiol*. 2010;72:219–246.
3. Schenk S, et al. Insulin sensitivity: modulation by nutrients and inflammation. *J Clin Invest*. 2008;118(9):2992–3002.
4. Suzuki MM, Bird A. DNA methylation landscapes: provocative insights from epigenomics. *Nat Rev Genet*. 2008;9(6):465–476.
5. Backdahl L, et al. Inflammatory signalling as mediator of epigenetic modulation in tissue-specific chronic inflammation. *Int J Biochem Cell Biol*. 2009;41(1):176–184.
6. Maunakea AK, et al. Epigenome mapping in normal and disease states. *Circ Res*. 2010;107(3):327–339.
7. Jeltsch A, Jurkowska RZ. New concepts in DNA methylation. *Trends Biochem Sci*. 2014;39(7):310–318.
8. Ito S, et al. Tet proteins can convert 5-methylcytosine to 5-formylcytosine and 5-carboxylcytosine. *Science*. 2011;333(6047):1300–1303.
9. He YF, et al. Tet-mediated formation of 5-carboxylcytosine and its excision by TDG in mammalian DNA. *Science*. 2011;333(6047):1303–1307.
10. Wang X, et al. Epigenetic regulation of macrophage polarization and inflammation by DNA methylation in obesity. *JCI Insight*. 2016;1(19):e87748.
11. Bock C, et al. Quantitative comparison of genome-wide DNA methylation mapping technologies. *Nat Biotechnol*. 2010;28(10):1106–1114.
12. Meissner A, et al. Reduced representation bisulfite sequencing for comparative high-resolution DNA methylation analysis. *Nucleic Acids Res*. 2005;33(18):5868–5877.
13. Smith ZD, et al. High-throughput bisulfite sequencing in mammalian genomes. *Methods*. 2009;48(3):226–232.
14. Monteiro R, et al. Estrogen signaling in metabolic inflammation. *Mediators Inflamm*. 2014;2014:615917.
15. Davis KE, et al. The sexually dimorphic role of adipose and adipocyte estrogen receptors in modulating adipose tissue expansion, inflammation, and fibrosis. *Mol Metab*. 2013;2(3):227–242.
16. Drew BG, et al. Estrogen receptor (ER)α-regulated lipocalin 2 expression in adipose tissue links obesity with breast cancer progression. *J Biol Chem*. 2015;290(9):5566–5581.

17. Jackson-Grusby L, et al. Loss of genomic methylation causes p53-dependent apoptosis and epigenetic deregulation. *Nat Genet*. 2001;27(1):31–39.
18. Eguchi J, et al. Transcriptional control of adipose lipid handling by IRF4. *Cell Metab*. 2011;13(3):249–259.
19. McCabe MT, et al. Inhibition of DNA methyltransferase activity prevents tumorigenesis in a mouse model of prostate cancer. *Cancer Res*. 2006;66(1):385–392.
20. Kaneda M, et al. Essential role for de novo DNA methyltransferase Dnmt3a in paternal and maternal imprinting. *Nature*. 2004;429(6994):900–903.
21. Liu XS, et al. Editing DNA methylation in the mammalian genome. *Cell*. 2016;167(1):233–247.
22. Vojta A, et al. Repurposing the CRISPR-Cas9 system for targeted DNA methylation. *Nucleic Acids Res*. 2016;44(12):5615–5628.
23. Saito K, et al. Progress in the molecular understanding of central regulation of body weight by estrogens. *Obesity (Silver Spring)*. 2015;23(5):919–926.
24. Hevener AL, et al. Impaired estrogen receptor action in the pathogenesis of the metabolic syndrome. *Mol Cell Endocrinol*. 2015;418 Pt 3(pt 3):306–321.
25. Campion J, et al. Individuality and epigenetics in obesity. *Obes Rev*. 2009;10(4):383–392.
26. Holness MJ, Sugden MC. Epigenetic regulation of metabolism in children born small for gestational age. *Curr Opin Clin Nutr Metab Care*. 2006;9(4):482–488.
27. Ling C, Groop L. Epigenetics: a molecular link between environmental factors and type 2 diabetes. *Diabetes*. 2009;58(12):2718–2725.
28. Maier S, Olek A. Diabetes: a candidate disease for efficient DNA methylation profiling. *J Nutr*. 2002;132(suppl 8):2440S–2443S.
29. Vel Szarc KS, et al. Nature or nurture: let food be your epigenetic medicine in chronic inflammatory disorders. *Biochem Pharmacol*. 2010;80(12):1816–1832.
30. Cao Q, et al. Inhibiting DNA methylation by 5-Aza-2'-deoxycytidine ameliorates atherosclerosis through suppressing macrophage inflammation. *Endocrinology*. 2014;155(12):4925–4938.
31. Yang X, et al. Epigenetic regulation of macrophage polarization by DNA methyltransferase 3b. *Mol Endocrinol*. 2014;28(4):565–574.
32. Shoelson SE, et al. Inflammation and insulin resistance. *J Clin Invest*. 2006;116(7):1793–1801.
33. Permana PA, et al. Macrophage-secreted factors induce adipocyte inflammation and insulin resistance. *Biochem Biophys Res Commun*. 2006;341(2):507–514.
34. Suganami T, et al. A paracrine loop between adipocytes and macrophages aggravates inflammatory changes: role of free fatty acids and tumor necrosis factor alpha. *Arterioscler Thromb Vasc Biol*. 2005;25(10):2062–2068.
35. Lumeng CN, et al. Macrophages block insulin action in adipocytes by altering expression of signaling and glucose transport proteins. *Am J Physiol Endocrinol Metab*. 2007;292(1):E166–E174.
36. Jurkowska RZ, et al. Structure and function of mammalian DNA methyltransferases. *Chembiochem*. 2011;12(2):206–222.
37. Fatemi M, et al. Dnmt3a and Dnmt1 functionally cooperate during de novo methylation of DNA. *Eur J Biochem*. 2002;269(20):4981–4984.
38. Kim GD, et al. Co-operation and communication between the human maintenance and de novo DNA (cytosine-5) methyltransferases. *EMBO J*. 2002;21(15):4183–4195.
39. Scherer PE, et al. A novel serum protein similar to C1q, produced exclusively in adipocytes. *J Biol Chem*. 1995;270(45):26746–26749.
40. Santos RS, et al. Activation of estrogen receptor alpha induces beiging of adipocytes. *Mol Metab*. 2018;18:51–59.
41. Zhou Z, et al. Estrogen receptor α controls metabolism in white and brown adipocytes by regulating *Polg1* and mitochondrial remodeling. *Sci Transl Med*. 2020;12(555):eaax8096.
42. Bartness TJ, Song CK. Thematic review series: adipocyte biology. Sympathetic and sensory innervation of white adipose tissue. *J Lipid Res*. 2007;48(8):1655–1672.
43. Bartness TJ, et al. Sympathetic and sensory innervation of brown adipose tissue. *Int J Obes (Lond)*. 2010;34(suppl 1):S36–S42.
44. Cao Q, et al. Sympathetic nerve innervation is required for beigeing in white fat. *Physiol Rep*. 2019;7(6):e14031.
45. Nguyen NL, et al. Separate and shared sympathetic outflow to white and brown fat coordinately regulates thermoregulation and beige adipocyte recruitment. *Am J Physiol Regul Integr Comp Physiol*. 2017;312(1):R132–R145.
46. Cao Y, et al. Whole-tissue 3D imaging reveals intra-adipose sympathetic plasticity regulated by NGF-TrkA signal in cold-induced beiging. *Protein Cell*. 2018;9(6):527–539.
47. Blaszkiewicz M, et al. Adipose tissue myeloid-lineage neuroimmune cells express genes important for neural plasticity and regulate adipose innervation. *Front Endocrinol (Lausanne)*. 2022;13:864925.
48. Cui X, et al. Adipose tissue-derived neurotrophic factor 3 regulates sympathetic innervation and thermogenesis in adipose tissue. *Nat Commun*. 2021;12(1):5362.
49. Miranda RC, et al. Interactions of estrogen with the neurotrophins and their receptors during neural development. *Horm Behav*. 1994;28(4):367–375.
50. Bimonte-Nelson HA, et al. Progesterone counteracts estrogen-induced increases in neurotrophins in the aged female rat brain. *Neuroreport*. 2004;15(17):2659–2663.
51. Bjorling DE, et al. Modulation of nerve growth factor in peripheral organs by estrogen and progesterone. *Neuroscience*. 2002;110(1):155–167.
52. Jezierski MK, Sohrabji F. Region- and peptide-specific regulation of the neurotrophins by estrogen. *Brain Res Mol Brain Res*. 2000;85(1–2):77–84.
53. Scharfman HE, MacLusky NJ. Estrogen and brain-derived neurotrophic factor (BDNF) in hippocampus: complexity of steroid hormone-growth factor interactions in the adult CNS. *Front Neuroendocrinol*. 2006;27(4):415–435.
54. Teng J, et al. Estrogen-induced proliferation of urothelial cells is modulated by nerve growth factor. *Am J Physiol Renal Physiol*. 2002;282(6):F1075–F1083.
55. You D, et al. Dnmt3a is an epigenetic mediator of adipose insulin resistance. *Elife*. 2017;6:e30766.
56. Park YJ, et al. DNMT1 maintains metabolic fitness of adipocytes through acting as an epigenetic safeguard of mitochondrial dynamics. *Proc Natl Acad Sci U S A*. 2021;118(11):e2021073118.
57. Yang X, et al. DNA methylation biphasically regulates 3T3-L1 preadipocyte differentiation. *Mol Endocrinol*. 2016;30(6):677–687.

58. Zha L, et al. The histone demethylase UTX promotes brown adipocyte thermogenic program via coordinated regulation of H3K27 demethylation and acetylation. *J Biol Chem*. 2015;290(41):25151–25163.
59. Li F, et al. Histone deacetylase 1 (HDAC1) negatively regulates thermogenic program in brown adipocytes via coordinated regulation of histone H3 lysine 27 (H3K27) deacetylation and methylation. *J Biol Chem*. 2016;291(9):4523–4536.
60. Cao Q, et al. Myeloid deletion of α1AMPK exacerbates atherosclerosis in LDL receptor knockout (LDLRKO) mice. *Diabetes*. 2016;65(6):1565–1576.
61. Pei L, et al. Genome-wide DNA methylation analysis reveals novel epigenetic changes in chronic lymphocytic leukemia. *Epigenetics*. 2012;7(6):567–578.